RSC Advances

ROYAL SOCIETY OF CHEMISTRY

www.rsc.org/advances

RSC Advances

PAPER

A General Protocol for π–conjugated Molecules–based Micro/nanospheres: Artificial Supramolecular Antenna in terms of Heterogeneous Photocatalysis

Received 00th January 20xx,
Accepted 00th January 20xx

DOI: 10.1039/x0xx00000x

www.rsc.org/

Xiao Zhang, Yanping Wang, Penglei Chen,* Peipei Guo, and Minghua Liu

The assembly of π–conjugated molecules–based supramolecular micro/nanostructures is acknowledged as a versatile platform correlating supramolecular chemistry and soft matter science, wherein those with a spherical morphology are a topic of general concern. Most of the existing protocols, however, work only in some specific scenarios. It still remains a formidable challenge to initiate a general protocol for supramolecular micro/nanospheres of desired π–conjugated molecules. We herein report our new findings that numerous porphyrins and some other π–conjugated molecules, including phthalocyanine, anthracene, and naphthalenediimide derivatives, could be assembled to form micro/nanospheres *via* an oil–in–water–mediated surfactant–assisted assembly. As an example for the functionalization of the as–assembled structures, we show that supramolecular light–harvesting antenna system with regard to photo–semiconductors–based heterogeneous photocatalysis could be achieved using porphyrin spheres. It is disclosed that the distinct chromophoric arrangements, which endow our porphyrin spheres with different photoinduced electron–hole separation capability, contribute greatly to their superior/inferior catalytic performances. Our new method might initiate a general way for advanced micro/nanospheres of desired π–conjugated molecules and desired functions.

Introduction

Π–conjugated molecules–based supramolecular micro/nanoassemblies of a well–defined morphology have been recognized to be a feasible forum bridging supramolecular chemistry and advanced materials science, as well–documented in recent review articles.[1–17] On one hand, this is owing to the rigid yet tunable geometry of π–conjugated molecules, which endow them with excellent assembly properties and thus render them promising candidates as ideal building blocks for the constructions of well–defined micro/nanostructured assemblies.[1–17] On the other hand, this stems from the aromatic electrons delocalized over the frame of π–conjugated molecules, as well as their readily tailored spectroscopic properties, which confer their micro/nanoassemblies with exceptional physicochemical, photochemical, and biological properties.[1–17] These characteristics provide π–conjugated molecules–based supramolecular micro/nanostructures with a wide variety of opportunities in numerous fields of paramount importance, including supramolecular electronics, light–harvesting and energy conversion systems, chemical/biological sensors, biomedicines, *etc.*[1–17]

During the past decades, a wide range of π–conjugated molecules–based supramolecular materials of a one–dimensional morphology have witnessed a huge progress in the development of advanced soft matters,[1–9] while those architectured with other morphologies, such as toroidal–, sheetlike–, and flowerlike structures,[10–17] especially those with a spherical morphology,[11–17] have also aroused ever–increasing attention and become an important topic of broad interest. This is promoted by their wide application possibilities as advanced functional soft materials in the fields of nonlinear optics, photocatalysts, antibacterial materials, drug delivery, *etc.*[11–17] So far, numerous spherically–shaped micro/nanoassemblies based on π–conjugated molecules have been successfully constructed by means of diverse strategies, including, but not confined to, mixed solvent–induced assembly, interfacial evaporization–condensation, coordination–assisted self–assembly, temperature–tuned assembly, *etc.*[11–17] Nevertheless, most of the current existing methods generally suffer from the requirement of elaborately–designed *ad–hoc* π–conjugated building blocks, which are commonly synthesized *via* a tedious and complex synthesis work.[11–17] Meanwhile, it sometimes is necessary that the assembly has to be performed with an accurate consideration of the experimental parameters, since only a slight change in the assembly conditions would lead to products of distinct or mixed morphologies.[11–17] It thus is strongly desired to launch a facile yet general protocol to produce spherical micro/nanostructures using desired π–conjugated molecules as building blocks.

Beijing National Laboratory for Molecular Science, Institute of Chemistry, Chinese Academy of Sciences, No. 2 Zhongguancun Beiyijie, Beijing 100190, People's Republic of China. E–mail: chenpl@iccas.ac.cn

† Electronic Supplementary Information (ESI) available: The UV–vis spectrum and SEM images of the TPP aggregates obtained using plain water as host solution, the real–time absorption spectra of RhB dye during the photodegradation process, and other related data. See DOI: 10.1039/x0xx00000x

To meet this formidable challenge, we herein report our new findings that the 5,10,15,20–Tetraphenylporphyrin (TPP, Fig. 1A), one of the most common commercial porphyrins, could be readily assembled to spherical structures *via* an oil–in–water–mediated surfactant–assisted self–assembly (SASA) under ambient conditions. We show that when a chloroform solution of TPP molecules is added into an aqueous solution of sodium dodecyl benzene sulfonate surfactant (SDBS, Fig. 1A), spherical TPP assemblies (Fig. 2) could be produced. Significantly, we further demonstrate that such simple protocol could be easily applied not only to numerous commercial porphyrins (Fig. 3), but also to some other π–conjugated molecules such as phthalocyanine, anthracene, and naphthalenediimide derivatives (Fig. 4). As an example for the potential functionalization of the as–assembled structures, we show that our spherical porphyrin assemblies could work as artificial supramolecular antenna in terms of heterogeneous photocatalysis. Among our spherical porphyrin micro/nanoassemblies, those based on TPP molecules display superior photocatalytic reactivity comparatively (Fig. 5). It is verified that the more efficient photoinduced electron–hole separation capability of the TPP spheres, which results from their higher content of J–aggregates, as well as the rough surface feature of the TPP spheres, which confers them with a more strong adsorption capability, contribute greatly to their superior photocatalytic performances.

The significance of our work is two–fold. First, taking into account the generally poor solubility of organic compounds in aqueous phase and their good solubility in oil phase, our oil–in–water–mediated SASA protocol might pave a facile yet general avenue for spherical micro/nanostructures of desired π–conjugated building blocks. Second, but not least, in view of the rich physicochemical properties of π–conjugated molecules, and the general interests of their supramolecular assemblies, our investigation might launch new and broad opportunities for advanced soft materials of a spherical morphology and of desired properties and uses.

Experimental section

Chemicals and reagents

5,10,15,20–tetraphenylporphyrin (TPP, Aldrich, >99%), 5,10,15,20–tetrakis(3,5–dimethoxyphenyl)porphyrin (TPPDOMe, TCI, >95%), 5–(4–carboxyphenyl)–10,15,20–triphenylporphyrin (TPPCOOH, TCI, >95%), 5–(4–methoxycarbonylphenyl)–10,15,20–triphenylporphyrin (TPPCOOMe, TCI, >90%), silicon 2,3,9,10,16,17,23,24–octakis(octyloxy)–29H,31H–phthalocyanine dihydroxide ($SiPc(OH)_2$, Aldrich, 95%), 2–aminoanthracene (NH_2AN, Aldrich, 96%), 4,9–dibromo–2,7–bis(2–octyldodecyl)benzo[lmn][3,8]phenanthroline–1,3,6,8(2H,7H)–tetraone (NDI, SunaTech Inc., 90%), sodium dodecyl benzene sulfonate (SDBS, TCI, >95%), cetyltrimethylammonium bromide (CTAB, Aldrich), and rhodamine B (RhB, Alfa Aesar) were used as received without further purification. 5, 5–dimethyl–1–pyrroline oxide (DMPO, Sigma Aldrich) was used as the electron spin resonance (ESR) spin–trapping reagents. Chloroform was used as the solvent for π–conjugated molecules, and ultrapure Milli–Q water (18 MΩ cm) was employed as the solvent for SDBS, CTAB, RhB, and DMPO.

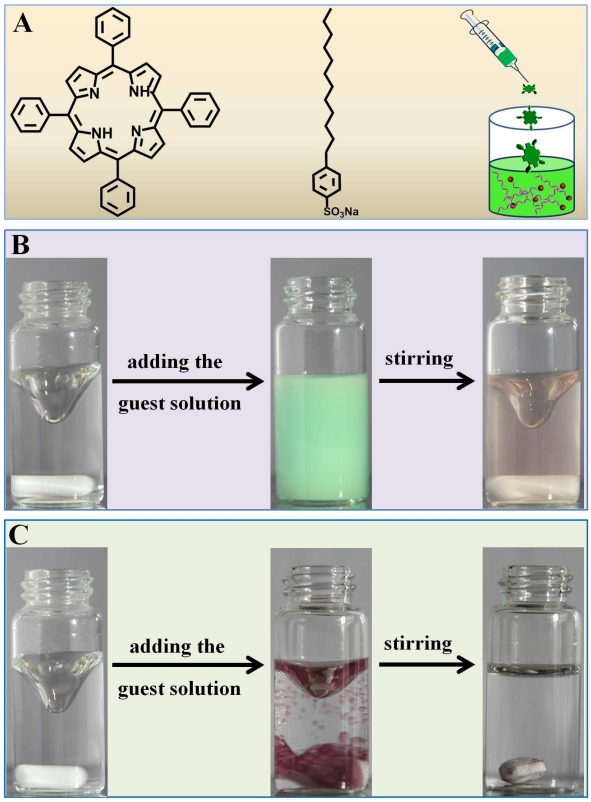

Fig. 1 A): Molecular structures of TPP and SDBS. B) and C): Typical digital pictures for our oil–in–water–mediated self–assembly of TPPs with the existence (B) and absence (C) of SDBS surfactant.

Assembly of spherical supramolecular micro/nanoassemblies *via* an oil–in–water–mediated SASA protocol

To fulfil the SASA experimentally, a chloroform solution (which served as the guest oil phase) of the desired π–conjugated molecules was dropwise added into an aqueous solution of SDBS surfactant (which worked as the host water phase) under ambient conditions with vigorous magnetic stirring. An opaque dispersion was obtained soon after the addition. With the evaporation of chloroform, the as–produced opaque dispersion became a transparent system gradually. The as–fabricated micro/nanostructures were then washed adequately with Milli–Q water *via* repeating centrifugations. As a typical example, the experimental procedure was elucidated by the assembly of TPP molecules as the followings. A chloroform solution of TPPs (2000 μL, 2×10^{-4} M) was dropped into an aqueous solution of SDBS surfactant (10 mL, 10 mM) under vigorous stirring, leading to the formation of a greenish opaque dispersion. After the magnetic stirring was performed for *ca.* 30 minutes for the evaporation of chloroform, a transparent dispersion could be produced. The as–assembled assemblies were washed fully with Milli–Q water by means of a couple of centrifugations (12000 rpm, 15 minutes). The as–obtained

products were then subjected to various characterizations or photocatalytic uses.

In the case of the controlled experiments, wherein plain Milli–Q water with no surfactant was used as the host solution, almost similar experimental procedure was carried out except that solid products either adsorbed on the stirring bar, or floating on the surface of the dispersion, are obtained after the evaporation of chloroform. These solid products were collected and subjected to SEM measurements.

Photocatalytic performances

In a typical photocatalytic experiment, spherical porphyrin assemblies (*ca.* 4×10^{-7} mol) were dispersed in an aqueous solution of RhB dye (4 mL, 10 mg L^{-1}). The dispersion was stirred for 30 minutes in a dark room to achieve an equilibrium adsorption, after which the catalytic experiment was carried out. A 500 W xenon arc lamp, installed in a laboratory lamp housing system (CHF–XM35–500 W, Beijing Trusttech Co. Ltd., China), was employed as the light source. Before entering the reactor (a quartz cuvette), the light passed through a 10 cm water filter and a UV cutoff filter (>420 nm). During the photocatalytic performances, an aliquot of the dispersion (0.3 mL) was taken out from the reaction system at an appointed time for real–time sampling. The samples were centrifugated (12000 rpm, 15 minutes), after which the UV–vis spectra of the supernate was measured. The photodegradation of RhB was monitored by measuring the real–time UV–vis absorption of RhB at 554 nm. For the evaluation of the photocatalytic reactivity, C was the concentration of RhB molecules at a real–time (t), and C_0 was that immediately before it was kept in dark room. The rate constant of the photocatalytic performances, in terms of the correlation between $\ln(C/C_0)$ and the reaction time t, was deduced by a kinetic linear simulation of the curves of the photocatalytic performances. For comparison, blank experiments without the involvement of spherical porphyrin assemblies were also performed in the similar way.

Apparatus and measurements

A JASCO UV–550 spectrophotometer was used for the measurements of UV–vis spectra. The scanning electron microscopy (SEM) measurements were performed by using a Hitachi S–4800 system. The energy–dispersive X–ray spectroscopy (EDX) was measured with a Horiba EMAX X–act energy–dispersive spectroscope that was attached to the Hitachi S–4800 system. Dynamic light scattering (DLS) measurements were conducted (Malvern, Nano ZS, ZEN3600) to investigate the particle size distribution of the as–produced spheres. The transmission electron microscopy (TEM) measurements were achieved using a JEOL TEM–2010 electron microscope (Japan) equipped with a charge–coupled device (CCD) camera. ESR investigations using DMPO as the spin–trapping reagents for the detection of reactive oxygen species were performed on a Brucker model EPR 300E spectrometer, which was equipped with a Quanta–Ray Nd:YAG laser (532 nm). The settings were as follows: center field = 3510.00 G, sweep width = 200.0 G and power = 10.02 mW. The ESR spectrometer was coupled to a computer for data acquisition and instrument control. For all ESR measurements, the same quartz capillary tube was used to minimize experimental errors.

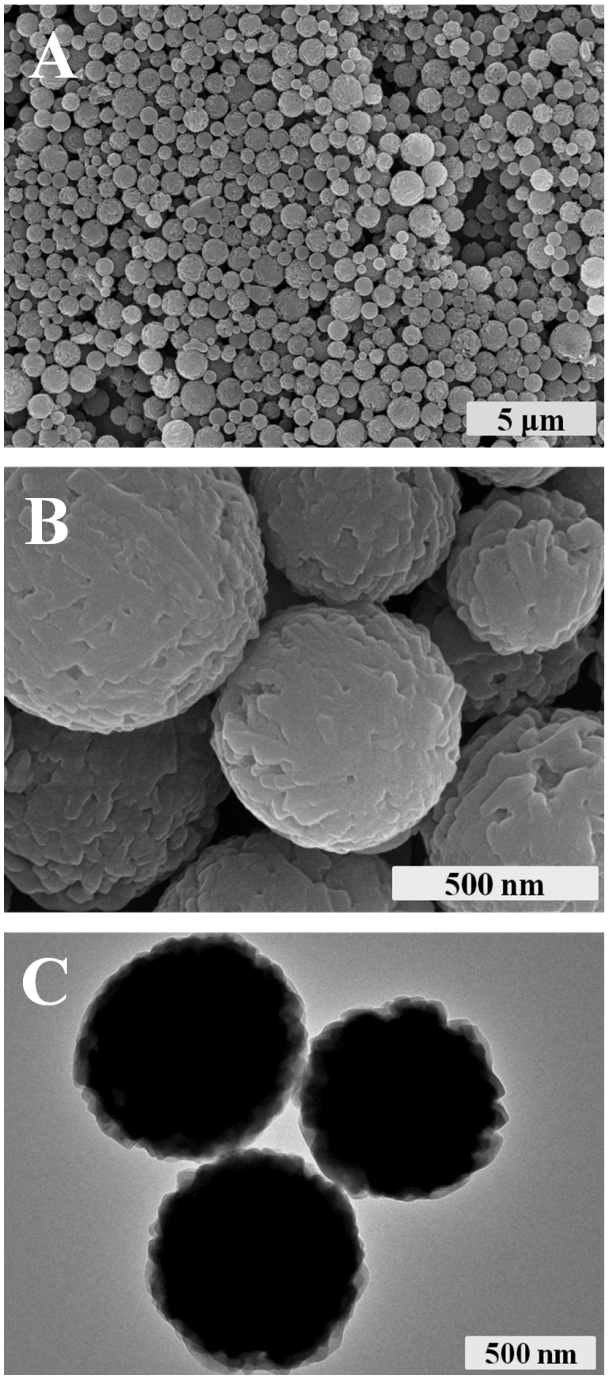

Fig. 2 A) and B): Low– (A) and high–magnification (B) SEM images of the spherical TPP structures *via* our oil–in–water–mediated SASA. C): TEM image of the as–assembled structures.

For photoelectrochemical experiments, indium tin oxide (ITO) glass electrodes were modified by our spherical porphyrin assemblies. To achieve this, *ca.* 4×10^{-7} mol porphyrin micro/nanospheres, which were dispersed in 1 mL water were coated onto a 2 cm × 2 cm ITO electrode and dried under ambient conditions. The photocurrent experiments were carried out in a

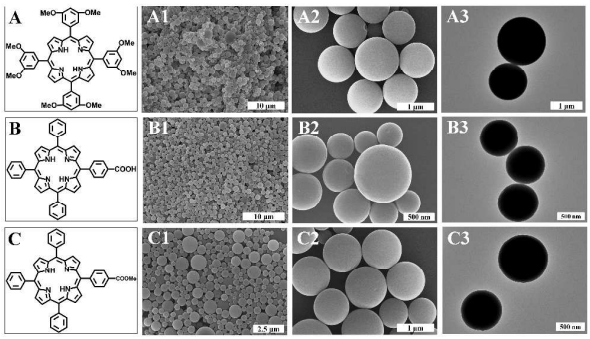

Fig. 3 A): Molecular structure of TPPDOMe. A1–A3): Low–(A1) and high–magnification (A2) SEM images, and TEM image (A3) of the spherical TPPDOMe structures *via* our oil–in–water–mediated SASA protocol. B–B3): The corresponding results for TPPCOOH. C–C3): The corresponding results for TPPCOOMe.

three–electrode system using ITO electrodes, which were modified by our porphyrin spheres, as the working electrode, and a platinum wire and a saturated calomel electrode (SCE) as the counter electrodes and the reference electrode, respectively. The potential of the working electrode was held at 0 V versus SCE during the measurements. An aqueous solution of Na_2SO4 (0.1 M) was used as the electrolyte. The working electrode was intermittently irradiated with visible–light during the measurements. Photocurrent–time characteristics were recorded with a CHI 660B electrochemical analyzer (Shanghai Chenhua Instrumental Co., Ltd., China). All of the measurements were carried out at room temperature.

Results and discussion

To accomplish the assembly experimentally, a chloroform solution of TPP molecuels (guest solution) was dropwise added into an aqueous solution of SDBS surfactant (host solution) under ambient conditions with vigorous magnetic stirring. As shown in Fig. 1B, a greenish opaque dispersion comes into being immediately after the addition of the guest solution. This dispersion gradually becomes a pink transparent system with the evaporation of chloroform. In contrast, when plain water with no surfactant is used as the host solution, a transparent dispersion, within which pink–colored oil phase is heterogeneously dispersed, could be obtained after the addition, as shown in Fig. 1C. In this case, after the evaporation of the dispersed chloroform phase, dark purple solids either adsorbed on the stirring bar or floating on the surface of the dispersion are obtained, while the transparent solution itself is nearly colorless. As shown in Fig. S1, the as–produced colorless dispersion exhibits only negligible absorptions, while the chloroform solution of TPP molecules displays distinct Soret band at *ca.* 419 nm. These experimental facts indicate that our TPP molecules could hardly be brought into aqueous phase by chloroform. This actually is reasonable, since the TPP molecuels are nearly water–insoluble species, and meanwhile, chloroform is unmixable with plain water. In comparison, the observations of the SDBS surfactant–involved system (Fig. 1B) suggest that our TPPs originally dissolved in the

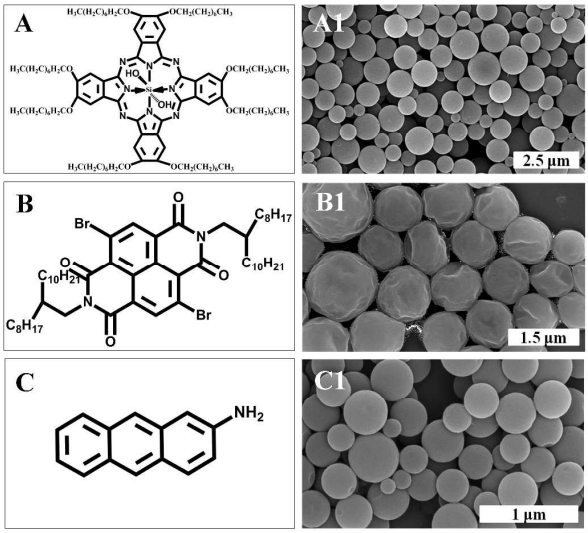

Fig. 4 A) and A1): Molecular structure of $SiPc(OH)_2$ (A) and the corresponding SEM image (A1) of the as–fabricated structures. B) and B1): Molecular structure of NDI (B) and the corresponding SEM image (B1) of the as–fabricated structures. C) and C1): Molecular structure of NH_2AN (C) and the corresponding SEM image (C1) of the as–fabricated structures.

chloroform oil phase could be implanted into aqueous phase with the assistance of SDBS surfactant.

The dispersions prepared in the SDBS system were treated by means of centrifugation, and the obtained precipitates were washed thoroughly with Milli–Q water by a couple of additional centrifugations, after which the produced solids were subjected to various characterizations. As shown in Fig. 2A, well–defined discrete spherical structures with a diameter of *ca.* 200 nm~1 μm were observed from the scanning electron microscopy (SEM) images of the samples. Such a broad particle size distribution could be confirmed by the DLS of the sample, as presented in Fig. S2. A close observation of the high–magnification SEM image of the samples indicates that the as–produced spheres, which are composed of sheetlike and/or one–dimensional nanospecies, have a rough surface, as illustrated in Fig. 2B. The formation of the spherical assemblies and their rough surface could be confirmed by transmission electron microscopy (TEM) image, as shown in Fig. 2C. The SEM image of our TPP spheres was also measured after the assembly systems were aged for 2 weeks (Fig. S3). It can be see that compared with the freshly fabricated spheres (Fig. 2A, 2B), the as–produced spheres display negligible changes in their morphology, indicating their good stability. In the case of the assembly system without the involvement of SDBS surfactant, the TPP aggregates absorbed on the stirring bar or floating on the surface of the dispersion were collected and their SEM images were also measured. As shown in Fig. S4, irregular structures instead of well–defined spherical structures are observed. These observations imply that our TPP molecules could not be organized to form well–defined supramolecular micro/nanostructures without the assistance of surfactants.

The component of our TPP spheres was investigated by EDX analysis. As shown in Fig. S5, except C and Si elements (note that the Si slice was used as solid support for the EDX measurements), negligible signals ascribing to S and Na elements, which are contained in the SDBS surfactant, could be detected. These facts indicate that the SDBS surfactant in our assembly system might mainly play a role of morphology template but not be involved in the self–assembly of TPP molecules themselves.

As it is widely known, an oil guest phase (*viz.* chloroform, in the present case) could be dispersed in an aqueous host phase with the assistance of surfactants, giving out a microemulsion system.[17–20] This is owing to the incompatibility of oil and water phases, and also owing to the intrinsic amphiphilicity feature of the surfactants, which spherically enwrap the oil guest phases and thus promote their disperse in water.[17–20] On the basis of these basic understandings, and together with the above–described experimental results, we can propose a plausible interpretation for the formation of spherically–shaped TPP structures. When a chloroform (oil) solution of our TPP molecules was dropped into an aqueous solution of SDBS surfactants, the oil phase was spherically dispersed in water with the assistance of the amphiphilic surfactant,[17–20] resulting in an opaque microemulsion system. Owing to their poor water–solubility, most of TPP molecules are locally confined in the spherical micro–oil phase rather than being transferred to the host water phase. At the same time, owing to the nice volatility of chloroform, the TPP molecules begin to self–assembly with the evaporation of chloroform. This leads to the formation of spherical TPP structures, which inherit the morphology of the spherically–shaped micro–oil phase.[17–20]

It can be seen that our oil–in–water–mediated SASA protocol might be an extremely easy way to manufacture spherical supramolecular assemblies using commercially available TPP molecules as building blocks, and such method might be based on an extremely simple mechanism. It thus is logical to question whether the method could be suitable for other commercial porphyrins or even for other π–conjugated molecules. In order to experimentally verify the generality of our facile method, some other commercial porphyrins (Fig. 3), including 5,10,15,20–tetrakis(3,5–dimethoxyphenyl)porphyrin (TPPDOMe), 5–(4–carboxyphenyl)–10,15,20–triphenylporphyrin (TPPCOOH), 5–(4–methoxycarbonylphenyl)–10,15,20–triphenylporphyrin (TPPCOOMe), were also assembled in the similar way. As shown in Fig. 3, spherical assemblies of a smooth surface and a diameter of *ca.* 200 nm~1 μm could be observed from the SEM and TEM images of the as–fabricated samples. With regard to DLS and EDX, similar results as those of the TPP spheres are obtained, as shown in Fig. S2 and S5, respectively. These results confirm that the formation of the spherical structures is directed by the surfactant–enwrapped spherically–shaped micro–oil phase in terms of inheriting their spherical morphology.[17–20] Importantly, this, to some extent, indicates the generality of our protocol.

Besides the above–mentioned porphyrins, the generality of our oil–in–water–mediated SASA protocol could be further experimentally confirmed by using several other commercial π–conjugated molecules (Fig. 4), for examples, the derivatives of phthalocyanine (silicon 2,3,9,10,16,17,23,24–octakis(octyloxy)–29H,31H–phthalocyanine dihydroxide, abbreviated as $SiPc(OH)_2$), naphthalenediimide (4,9–dibromo–2,7–bis(2–octyldodecyl)benzo[lmn][3,8]phenanthroline–1,3,6,8(2H,7H)–tetraone, abbreviated as NDI), and anthracene (2–aminoanthracene, abbreviated as NH_2AN). As shown in Fig. 4, similar to the cases of

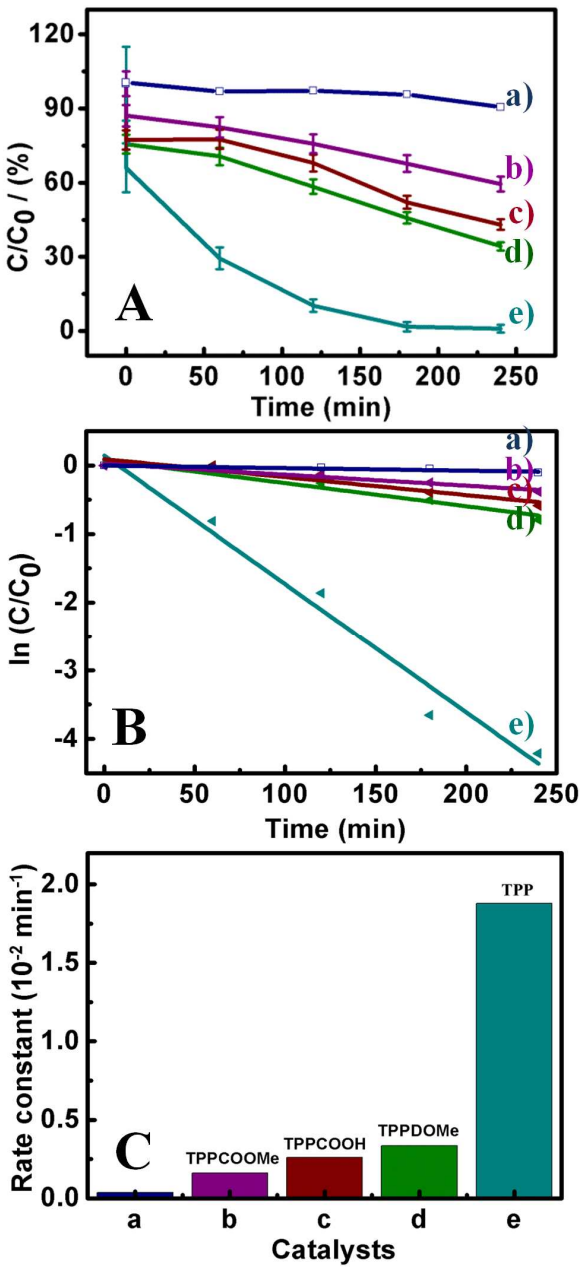

Fig. 5 Photocatalytic performances (A), kinetic linear simulation curves (B), and the corresponding histogram of the reaction rate constants (C) of our porphyrin spheres–based photocatalysts towards RhB degradation. The catalysts are the spherical TPPCOOMe (b), TPPCOOH (c), TPPDOMe (d), and TPP (e) structures, respectively. The result obtained from a blank experiment (a) without the involvement of the catalysts is also presented for comparison.

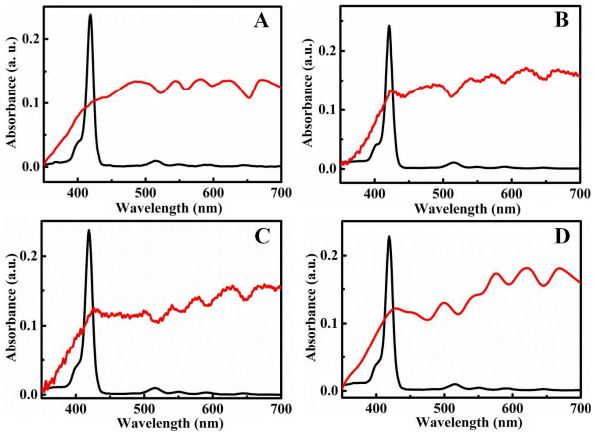

Fig. 6 UV–vis spectra of TPP (A), TPPDOMe (B), TPPCOOH (C), and TPPCOOMe (D) dissolved in chloroform solution (black curves), and those of the corresponding spherical structures (red curves).

our porphyrins (Fig. 2 and 3), all of these π–conjugated molecules could also be facilely assembled to form spherical micro/nanostructures *via* the similar SASA process. Moreover, the generality of our SASA strategy could also be verified by the effect of the concentration of the surfactant host solution and the type of the employed surfactant. Taking the assembly of TPP as a typical example, it was found that spherical structures could be produced when the concentration of the employed SDBS host solution was changed from 1.25 mM to 20 mM, as representatively shown in Fig. S6A and S6B. Moreover, taking the assembly of TPPDOMe as a representative paradigm, we investigated the effect of different surfactants, wherein a cetyltrimethylammonium bromide (CTAB) aqueous solution is used as the host solution. As shown in Fig. S7, spherical structures could be also obtained. These issues further confirm the generality of our protocol for the formulation of spherical structures of π–conjugated molecules.

Of various π–conjugated molecules, porphyrins, which are often referred to as *'the pigments of life'*, have received particular expectations from the interdisciplinary communities of supramolecular chemistry and advanced soft matter science.[11–16, 21] This is promoted by: (i) their well understood geometric structures, as well as their featured visible–light spectroscopy make them versatile components for well–defined and characteristic advanced supramolecular materials of fertile physicochemical properties;[11–16, 21] (ii) their built–in capability to mimic biological processes, such as photosynthesis and photorespiration, makes them ideal model scientific forum for the primary research on the performance of light–harvesting antenna system occurring in natural ecosystems.[12, 15, 21–24] The latter issue is specially significant, since it might launch great opportunities for light energy conversion in terms of photocatalysis, photodynamic therapy, photovoltaics, and optoelectronics, *etc.*[12, 15, 21–24] Here, as an example for the potential functionalization of our porphyrin spheres, their photocatalytic performances in terms of the visibile–light–driven photocatalytic degradation of rhodamine B (RhB) were investigated.[25] The photocatalytic process was monitored by means of measuring the real–time UV–vis absorption of RhB molecules at a wavelength of 554 nm.

As shown in Fig. 5A, and S8A, when no catalysts are involved in the reaction system, negligible photodegradation of RhB molecules could be achieved under visible–light irradiation. This suggests that the self–photosensitized decomposition of RhB molecules under our experimental conditions could be substantially ignored. On the other hand, when our porphyrin spheres are introduced into the reaction systems, evident decomposition of RhB molecules could be observed, as shown in Fig. 5 and Fig. S8B–S8E. These results indicate that the as–formulated spherical porphyrin structures could work as heterogeneous photocatalysts for the photodegradation of RhB molecules.[25] Specifically speaking, as shown in Fig. 5A and Fig. S8B–S8D, *ca.* 41%, 57%, and 66% RhB molecules are photodecomposed within 240 minutes, respectively, when our TPPCOOMe, TPPCOOH, and TPPDOMe spheres are employed as photocatalysts.

The rate constants of the photocatalytic reactions in terms of the correlation between $\ln(C/C_0)$ and the reaction time (t) were extracted by a kinetic linear simulation of the photocatalytic performance curves. As plotted in Fig. 5B, there is a nice linear correlation between $\ln(C/C_0)$ and t. This implies that the photodegradation reaction of RhB molecules over our pophyrin spheres–based photocatalysts follows the first–order kinetics. The rate constants of the photocatalytic reactions over our TPPCOOMe, TPPCOOH, and TPPDOMe spheres are *ca.* $(1.60\pm0.14) \times 10^{-3}$, $(2.61\pm0.09) \times 10^{-3}$, and $(3.36\pm0.36) \times 10^{-3}$ min^{-1}, respectively, indicating their comparable photocatalytic reactivity, as shown in Fig. 5B and 5C. Significantly, in the case of the TPP spheres–catalyzed system, a rate constant as high as *ca.* $(18.78\pm4.60) \times 10^{-3}$ min^{-1} is obtained. As shown in Fig. 5C, it can be seen that compared to that of the TPPCOOMe, TPPCOOH, and TPPDOMe spheres, the catalytic reactivity of our TPP spheres is substantially enhanced by a factor of *ca.* 11.7±3.9, 7.2±2.0, and 5.6±2.0, respectively. These results indicate that among our spherical porphyrin structures, TPP spheres are relatively superior visible–light–driven photocatalysts towards the photodegradation of RhB molecules. The recyclability of our TPP spheres–based photocatalysts was also investigated. As shown in Fig. S9, it is found that the photocatalytic performances display only a slight decrease without significant loss of activities after the reaction is performed consecutively 3 times. On the other hand, our results showed that compared with the newly fabricated samples (Fig. 2A, 2B), our TPP spheres exhibited negligible changes in their morphology after the catalytic performance (Fig. S10). These facts suggest that our TPP nanospheres could work as stable photocatalysts.

As it is known, the adsorption capability of a catalyst towards the substrate molecules is generally one of the critical factors that might affect its catalytic reactivity, wherein the higher is the adsorption capability, the higher is the catalytic performance.[26–28] The adsorption behaviors of our TPP spheres toward RhB molecules were investigated in terms of measuring the real–time UV–vis spectra of the catalytic system in a dark room during a period of 48 hours. As shown in Fig. S11, the absorption reached an equilibrium state after 30 minutes. Together with the photocatalytic results shown in Fig. 5, these results demonstrated that the drop in the

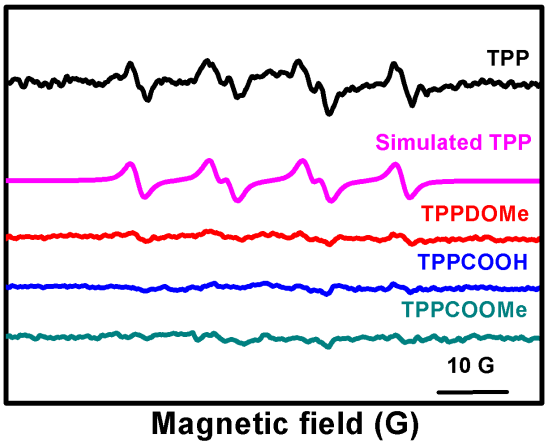

Fig. 7 ESR spectra of the of the DMPO–superoxide anion spin adducts generated in an aqueous solution containing TPP (black), TPPDOMe (red), TPPCOOH (blue), and TPPCOOMe (cyan) spherical structures, respectively. The simulated spectrum of the TPP system (magenta) obtained by a computer analysis is also presented.

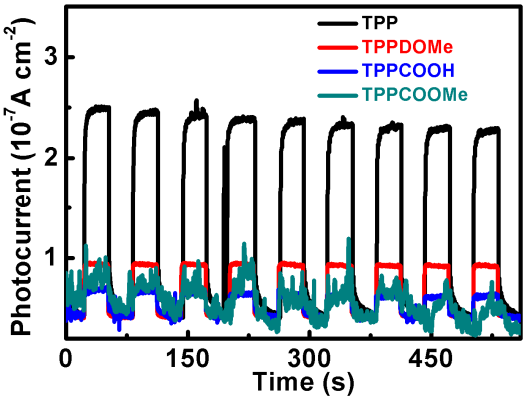

Fig. 8 Transient photocurrent responses of the ITO electrodes modified by our TPP (black), TPPDOMe (red), TPPCOOH (blue), and TPPCOOMe (cyan) spherical structures. The illumination was periodically interrupted every 30 seconds during the measurements.

visible absorption of RhBs during the catalytic performances was owing to the photodegradation of RhBs but not to their adsorption on the TPP spheres. As shown in Fig. 5A and S8, compared to the other three cases, our TPP spheres show a higher adsorption capability towards RhBs molecules. This could be ascribed to the rough surface features of the TPP spheres (Fig. 2B, and 2C), which might provide them with more adsorption sites. We suggest that this issue might contribute partially to the superior photocatalytic performances of our TPP spheres.

On the other hand, in addition to a higher adsorption capability, it is widely acknowledged that the performances of a photocatalyst could also be essentially promoted by an efficient photoinduced electron–hole separation.[26–30] In the case of the photosynthetic light–harvesting antenna system based on the assemblies of π–conjugated molecules, the stacking of the chromophoric building blocks in terms of J–aggregates, wherein the chromophores are coherently arranged with a slipped cofacial arrangement,[31–34] has been proved to be an useful scaffold that faciliates an efficient photoinduced electron–hole separation.[25, 31, 32, 35–38] This is owing to the existence of strong intermolecular π electronic coupling between the cooperatively arranged chromophores of J–aggregates, in which the delocalized π electrons coherently span over the slipped cofacial chromophores.[31–34] These issues render porphyrin–based J–aggregates feasible organic photo–semiconductors to mimic the light–harvesting antenna and photosynthetic performances of the chlorosomal rods, wherein photoinduced electron–hole separation is facilitated by the tightly coupled π–conjugated electrons of the closely packed porphyrin chromophores.[25, 35–38]

In order to disclose the different catalytic reactivity of our porphyrin spheres, the arrangement of their chromophores was investigated by UV–vis spectra. As shown in Fig. 6A, in the case of the monomeric TPP molecules dissolved in chloroform solution, a sharp Soret–band at *ca.* 419 nm and four Q–bands at *ca.* 514, 550, 591 and 643 nm are observed. Upon the formation of spherical structures, the Q–bands red–shifted to *ca.* 545, 580, 623, and 670 nm, respectively. Notably, the Soret–band in this case manifested itself as a broadened yet evidently red–shifted absorption maximum at *ca.* 490 nm, while that of the monomeric TPP molecules appeared only as a discernible shoulder peak of a weak profile. According to the exciton coupling model proposed by Kasha *et al*,[39, 40] it is widely known that the bathochromically–shifted and broadened Soret–band of porphyrins correspond to the formation of various nonspecific J–aggregates.[39–42] The above experimental facts accordingly indicate that most of our TPP chromophores are arranged as nonspecific J–type aggregates in the formed spheres,[41, 42] which could promote an efficient photoinduced electron–hole separation,[25, 31, 32, 35–38] and consequently endow our TPP spheres with superior photocatalytic performances.[25, 35]

On the other hand, as shown in Fig. 6B–6D, the UV–vis spectra of the other three porphyrin spheres exhibit almost similar patterns as those of the TPP spheres, except that (i) compared to the case of the TPP spheres, the absorption of the monomeric chromophores and the J–aggregates of these three spheres exhibited nearly comparable intensity; (ii) instead of a shoulder profile, the absorption of the monomeric chromophores of these spheres, which is readily distinguished from the red–shifted Soret–band, appeared as a relative sharp peak. These observations suggest the existence of nonspecific J–aggregates in these three spheres.[39–42] Meanwhile, it indicates that the content of the formed J–aggregates, however, is lower than the case of TPP spheres. For TPPDOMe molecules, this could be owing to the existence of two methoxyl groups on each of their phenyl units, which could bring about steric hindrance between the neighboring molecules. This disfavors the coherent slipped cofacial arrangement of the chromophores, and thus suppresses the formation of J–aggregates. For TPPCOOH and TPPCOOMe molecules, besides the steric hindrance effect brought about by the carboxyl or methoxycarbonyl groups, their asymmetric molecular architecture could also be an important factor that

hinders the formation of J–aggregates.[43] The existence of lower content of J–aggregates disfavors an efficient photoinduced electron–hole separation,[25, 31, 32, 35–38] and thus confers these three porphyrin spheres with inferior catalytic performances comparatively.

Generally, various reactive oxygen species (ROS) such as superoxide anion radical ($O_2^{\bullet-}$), hydrogen peroxide (H_2O_2), or hydroxyl radical (•OH) *etc.* might be involved during the performances of photocatalysts.[25, 27, 29, 30] To support our proposals, the possible generation of ROS in our photocatalytic systems were investigated by an electron spin resonance (ESR) spin–trapping method, wherein 5,5–dimethyl–1–pyrroline N–oxide (DMPO) was used as the spin–trapping reagent. As shown in Fig. 7 (black curve), a typical ESR spectrum characteristic of DMPO–$O_2^{\bullet-}$ spin adducts could be evidently observed from the TPP spheres system. A computer analysis and simulation of this ESR curve (Fig. 7, magenta curve) shows that the DMPO–$O_2^{\bullet-}$ spin adducts nearly account for 90% of the spectrum, wherein the hyperfine coupling constant values of α_N = 13.96 G, and α^{β}_{H} = 11.64 G are in good agreement with those reported by others.[44–46] These facts indicate the generation of superoxide anion radicals in the TPP spheres system, verifying an efficient photoinduced electron–hole separation, which favors a superior photocatalytic reactivity (Fig. 5). On the other hand, as shown in Fig. 7 (red, blue and cyan curves), only negligible ESR signals that resulted from the DMPO–$O_2^{\bullet-}$ spin adducts could be detected from the other three systems. These results are in good accordance with the different photocatalytic performances of our porphyrin spheres (Fig. 5). It confirms that compared to the TPP spheres, the other three porphyrin counterparts have a less capability for the generation of $O_2^{\bullet-}$ species, verifying a less efficient photoinduced electron–hole separation, and thus leading to their inferior photocatalytic reactivity (Fig. 5).

The more efficient photoinduced electron–hole separation capability of our TPP spheres compared to the other three counterparts were also examined in terms of photocurrent–time response (*I*–*t*) curves by means of their transient photocurrent responses under intermittent visible–light illumination. The photocurrent experiments were achieved using a three–electrode system, in which indium tin oxide (ITO) glasses modified by our porphyrin spheres were used as working electrodes. As shown in Fig. 8, it can be seen that for all of our porphyrin spheres, the photocurrent increases when light is switched on, while it decreases when light is switched off. Such reversible photocurrent responses could be performed repeatedly during the light switch on/off cycles. These observations indicate the separation and transportation of the photogenerated electron–hole pairs[47, 48] in our porphyrin spheres upon light irradiation. In the cases of the ITO electrodes modified by our TPPDOMe, TPPCOOH and TPPCOOMe spheres, relatively weak but comparable photocurrent responses could be observed (Fig. 8, red, blue and cyan curves). In contrast, the ITO electrodes modified by our TPP spheres display an evidently boosted photocurrent response under the similar experimental conditions (Fig. 8, black curve). These observations are in good agreement with the fact that compared to the other three porphyrin spheres, the TPP counterparts have a relatively stronger $O_2^{\bullet-}$ generation capability (Fig. 7) and could display superior photocatalytic performances (Fig. 5). Accompanied by the information deduced from the UV–vis (Fig. 6) and ESR (Fig. 7) spectra, these results further confirm that the more efficient photoinduced electron–hole separation in the TPP spheres, which is promoted by the formation of a higher content of J–aggregates, might play an important role for their superior photocatalytic performances.

Conclusions

In summary, we demonstrate that numerous π–conjugated molecules, including a series of commercial porphyrins, and derivatives of phthalocyanine, anthracene and naphthalenediimide could be facilely organized to form spherical micro/nanostructures by means of a SASA method, wherein an oil–in–water system is used as the assembly medium. In view of the generally good solubility of organic compounds in oil phase and their poor solubility in aqueous phase, our oil–in–water–mediated SASA protocol might initiate a general way for spherical supramolecular micro/nanostructures of desired π–conjugated molecules. We further show that artificial supramolecular light–harvesting antenna system based on our spherical porphyrin assemblies could be realized in terms of heterogeneous photocatalytic performances, wherein the TPP spheres display superior photocatalytic reactivity comparatively. Besides their different adsorption capability, the distinct molecular arrangement states, which endow these porphyrin assemblies with different photoinduced electron–hole separation capability, might play an important role for the different photocatalytic reactivity. Considering the rich physicochemical properties of π–conjugated molecules, and the general interests of their supramolecular assemblies, our SASA protocol might launch new and broad opportunities for advanced soft materials of a spherical morphology and of desired properties and functions.

Acknowledgements

We acknowledge the financial support from the National Natural Science Foundation of China (Grants 21372225, 20873159, 21321063, and 91027042), the National Key Basic Research Project of China (Grants 2013CB834504 and 2011CB932300), and the Chinese Academy of Sciences (Grants XDA09030200 and 1731300500015).

Notes and references

1 R. Li, W. Hu, Y. Liu and D. Zhu, *Acc. Chem. Res.,* 2010, **43,** 529–540.
2 H.–J. Kim, T. Kim and M. Lee, *Acc. Chem. Res.,* 2011, **44,** 72–82.
3 Y. Yan, Y. Lin, Y. Qiao and J. Huang, *Soft Matter,* 2011, **7,** 6385–6398.
4 L. Zang, Y. Che and J. S. Moore, *Acc. Chem. Res.,* 2008, **41,** 1596–1608.
5 J. P. Hill, L. K. Shrestha, S. Ishihara, Q. Ji and K. Ariga, *Molecules,* 2014, **19,** 8589–8609.
6 K. Sakakibara, J. P. Hill and K. Ariga, *Small,* 2011, **7,** 1288–1308.

7 F. S. Kim, G. Ren and S. A. Jenekhe, *Chem. Mater.,* 2011, **23,** 682–732.
8 D. González–Rodríguez and A. P. H. J. Schenning, *Chem. Mater.,* 2011, **23,** 310–325.
9 T. Niu, J. L. Zhang, W. Chen, (Eds: N.Koch), Royal Society of Chemistry, Cambridge, England, 2014, Ch. 3.
10 Y. Kim, W. Li, S. Shin and M. Lee, *Acc. Chem. Res.,* 2013, **46,** 2888–2897.
11 S. S. Babu, H. Möhwald and T. Nakanishi, *Chem. Soc. Rev.,* 2010, **39,** 4021–4035.
12 C. J. Medforth, Z. Wang, K. E. Martin, Y. Song, J. L. Jacobsen and J. A. Shelnutt, *Chem. Commun.,* 2009, 7261–7277.
13 Y. Li, T. Liu, H. Liu, M.–Z. Tian and Y. Li, *Acc. Chem. Res.,* 2014, **47,** 1186−1198.
14 H. Liu, J. Xu, Y. Li and Y. Li, *Acc. Chem. Res.,* 2010, **43,** 1496−1508.
15 T. Hasobe, *J. Phys. Chem. Lett.,* 2013, **4,** 1771−1780.
16 K. Ariga, T. Nakanishi and J. P. Hill, *Curr. Opin. Colloid Interface Sci.,* 2007, **12,** 106–120.
17 J. Pecher and S. Mecking, *Chem. Rev.,* 2010, **110,** 6260–6279.
18 Q. Chen, X. Shen and H. Gao, *Adv. Colloid Interface Sci.,* 2010, **159,** 32−44.
19 K. Margulis–Goshen and S. Magdassi, *Curr. Opin. Colloid Interface Sci.,* 2012, **17,** 290–296.
20 R. Dong, W. Liu and J. Hao, *Acc. Chem. Res.,* 2012, **45,** 504–513.
21 C. Zhang, P. Chen, H. Dong, Y. Zhen, M. Liu and W. Hu, *Adv. Mater.,* 2015, DOI: 10.1002/adma.201501273.
22 C. M. Drain, A. Varotto and I. Radivojevic, *Chem. Rev.,* 2009, **109,** 1630–1658.
23 J. A. A. W. Elemans, R. V. Hameren, R. J. M. Nolte and A. E. Rowan, *Adv. Mater.,* 2006, **18,** 1251–1266.
24 Y. Nakamura, N. Aratani and A. Osuka, *Chem. Soc. Rev,.* 2007, **36,** 831–845.
25 P. Guo, P. Chen, W. Ma and M. Liu, *J. Mater. Chem.,* 2012, **22,** 20243–20249.
26 M. Zhu, P. Chen and M. Liu, *ACS Nano,* 2011, **5,** 4529–4536.
27 C. Chen, W. Ma and J. Zhao, *Chem. Soc. Rev.,* 2010, **39,** 4206–4219.
28 M. Zhu, P. Chen and M. Liu, *Langmuir,* 2012, **28,** 3385−3390.
29 M. R. Hoffmann, S. T. Martin, W. Choi and D. W. Bahnemann, *Chem. Rev.,* 1995, **95,** 69−96.
30 A. L. Linsebigler, G. Lu and J. T. Yates. Jr., *Chem. Rev.,* 1995, **95,** 735−758.
31 F. Würthner, T. E. Kaiser and C. R. Saha–Möller, *Angew. Chem. Int. Ed.,* 2011, **50,** 3376−3410.
32 A. Satake and Y. Kobuke, *Org. Biomol. Chem.,* 2007, **5,** 1679–1691.
33 H. Kano and T. Kobayashi, *J. Chem. Phys.,* 2002, **116,** 184–195.
34 J. H. Van Esch, M. C. Feiters, A. M. Peters and R. J. M. Nolte, *J. Phys. Chem.,* 1994, **98,** 5541–5551.
35 P. Guo, P. Chen and M. Liu, *ACS Appl. Mater. Interfaces,* 2013, **5,** 5336−5345.
36 B. A. Friesen, B. Wiggins, J. L. McHale, U. Mazur and K. W. Hipps, *J. Am. Chem. Soc.,* 2010, **132,** 8554–8556.
37 A. D. Schwab, D. E. Smith, B. Bond–Watts, D. E. Johnston, J. Hone, A. T. Johnson, J. C. de. Paula and W. F. Smith, *Nano Lett.,* 2004, **4,** 1261–1265.
38 H. Kano, T. Saito and T. Kobayashi, *J. Phys. Chem. B,* 2001, **105,** 413–419.
39 M. Kasha, H. R. Rawls and M. A. El–Bayoumi, *Pure Appl. Chem.,* 1965, **11,** 371–392.
40 M. H. J. Wijnen, *J. Chem. Phys.,* 1958, **28,** 271–277.
41 Y. Zhang, P. Chen and M. Liu, *Chem. Eur. J.,* 2008, **14,** 1793–1803.
42 P. Guo, G. Zhao, P. Chen, B. Lei, L. Jiang, H. Zhang, W. Hu and M. Liu, *ACS Nano,* 2014, **8,** 3402–3411.
43 M. H. V. Reddy, R. M. Al–Shammari, N. Al–Attar, E. Kennedy, L. Rogers, S. Lopez, M. O. Senge, T. E. Keyes and J. H. Rice, *Phys. Chem. Chem. Phys.*, 2014, **16,** 4386–4393.
44 P. J. Bilski, M. A. Wolak, V. Zhang, D. E. Moore and C. F. Chignell, *Photochem. Photobiol.,* 2009, **85,** 1327–1335.
45 B. Zhao, K. Ranguelova, J. Jiang and R. P. Mason, *Free Radic. Biol. Med.,* 2011, **51,** 153–159.
46 G. Liu, S. Zheng, X. Xing, Y. Li, D. Yin, Y. Ding and W. Pang, *Chemosphere,* 2010, **78,** 402–408.
47 X. Zhang, M. Zhu, P. Chen, Y. Li, H. Liu, Y. Li and M. Liu, *Phys. Chem. Chem. Phys.,* 2015, **17,** 1217–1225.
48 Y. Wang, P. Chen, Y. Shen, C. Chen, C. Yang and M. Liu, *Phys. Chem. Chem. Phys.,* 2015, DOI: 10.1039/C5CP03618F.

Graphical Abstract

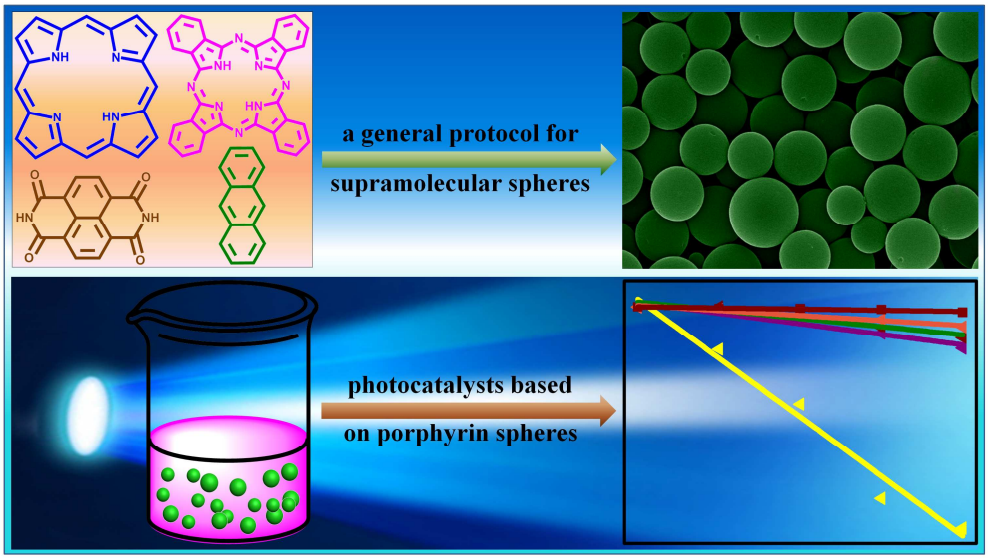

An oil-in-water-mediated surfactant-assisted assembly is initiated as a general method for π-conjugated molecules-based micro/nanospheres, supramolecular antenna with regard to heterogeneous photocatalysis has been realized using porphyrin spheres.